High-performance, ceria-based solid oxide fuel cells fabricated at low temperatures

Zhangbo Liu, Dong Ding, Mingfei Liu, Xifeng Ding, Dongchang Chen, Xiaxi Li, Changrong Xia, Meilin Liu

PII: S0378-7753(13)00740-4

DOI: 10.1016/j.jpowsour.2013.04.130

Reference: POWER 17298

To appear in: *Journal of Power Sources*

Received Date: 8 March 2013

Revised Date: 23 April 2013

Accepted Date: 25 April 2013

Please cite this article as: Z. Liu, D. Ding, M. Liu, X. Ding, D. Chen, X. Li, C. Xia, M. Liu, High-performance, ceria-based solid oxide fuel cells fabricated at low temperatures, *Journal of Power Sources* (2013), doi: 10.1016/j.jpowsour.2013.04.130.

Research Highlights:

- Single cells are fabricated at low temperatures with dense SDC electrolyte by co-pressing;
- The cell fabricated at 1150^{o}C shows higher performance than those made at higher temperatures;
- Adequate long-term stability is demonstrated for the cell fabricated at 1150^{o}C;
- Electrode polarization at high current densities is significantly suppressed at 650^{o}C.

High-performance, ceria-based solid oxide fuel cells fabricated at low temperatures

Zhangbo Liu[a, b, †], Dong Ding[a, †], Mingfei Liu[a, †], Xifeng Ding[a, c], Dongchang Chen[a], Xiaxi Li[a], Changrong Xia[b], Meilin Liu[a, *]

[a] *School of Materials Science and Engineering, Center for Innovative Fuel Cell and Battery Technologies, Georgia Institute of Technology,771 Ferst Drive NW, Atlanta, GA 30332, United States*

[b] *CAS Key Laboratory of Materials for Energy Conversion, Department of Materials Science and Engineering, University of Science and Technology of China, Hefei, 230026 Anhui, China*

[c] *School of Materials Science and Engineering, Nanjing University of Science and Technology, Nanjing, 210094 Jiangsu, China*

† These authors contribute equally to this work.

*****_E-mail:_ meilin.liu@mse.gatech.edu, _Tel:_ 404-894-6114, _Fax:_ 404-894-9140

Abstract

To reduce the fabrication cost and avoid unfavorable reactions between components of solid oxide fuel cells, it is necessary to improve the sinterability of the electrolyte materials, especially doped ceria for intermediate temperature operation. Here we report a unique process for fabrication of single cells at a co-sintering temperature as low as 1150^{o}C using highly active SDC powders derived from a glycine-nitrate process, demonstrating higher cell performance than those co-sintered at higher temperatures while maintaining adequate long-term stability. In particular, it is found that the electrode polarization at high current densities is significantly suppressed when operated at 650^{o}C.

Keywords: Ceria, Sintering, Electrolyte, Electrode, Solid oxide fuel cell.

Acronyms Used

DCO	doped ceria
GDC	gadolinia doped ceria
GNP	glycine-nitrate process
IT-SOFC	intermediate temperature solid oxide fuel cell
OCV	open cell voltage
SDC	samaria doped ceira
SOFC	solid oxide fuel cell
SSC	$Sm_{0.5}Sr_{0.5}CoO_3$
TPB	triple-phase boundary

1. Introduction

Solid oxide fuel cells (SOFCs) have potential to be the cleanest and the most efficient devices for cost-effective conversion to electricity of a wide variety of fuels, including hydrogen, hydrocarbons, coal gas, and bio-derived renewable fuels [1-7]. In recent years, intermediate temperature (500~700^{o}C) SOFCs (IT-SOFCs) have received much attention due to their improved stability, reliability, and materials selectivity compared with those to be operated at higher temperatures (≥800^{o}C) [8-11]. Doped ceria (DCO), particularly samaria doped ceria (SDC) and gadolinia doped ceria (GDC), are considered as the most promising electrolyte materials for IT-SOFCs, due to their superior ionic conductivity at reduced temperatures, higher catalytic activity for both oxygen reduction and fuel reforming, better compatibility with

cobalt-based cathodes, as well as closer thermal expansion coefficient to that of Ni-cermet anodes and ferrite stainless steel interconnects [12-18].

However, one of the main drawbacks of DCO-based materials is their poor sinterability, making it difficult to achieve sufficiently high density below 1500^{o}C [19-21]. The required high firing temperature of the electrolyte would result in a series of problems such as undesired grain growth and interfacial diffusions/reactions between the electrolyte and the electrode during co-firing, which are detrimental to cell performance and stability. Thus, many efforts have been devoted to improving the sinterability of DCO powders in order to effectively reduce the firing temperature, to optimize the electrode microstructure, and to minimize or eliminate unfavorable diffusion and reaction between cell components. One approach is to add a small amount of sintering aids such as MnO_2, Fe_2O_3, Co_3O_4, and Li_2O [22-32]. Another strategy is to develop unique processes for synthesis of ultra-fine DCO powders with higher sinterability, including hydrothermal synthesis, sol-gel, co-precipitation, intensive mechanical milling, and chemical combustion synthesis [15, 33-40].

In our recent work, a modified glycine-nitrate process (GNP) using 75 mol% $Ce(NO_3)_3$+25 mol% $Ce(NH_4)_2(NO_3)_6$ as a mixed cerium source was developed to synthesize SDC powders of highly sinterability with very low apparent tap density of only 36.0±0.5 mgcm^{-3}. Extremely dense SDC electrolyte membranes were fabricated from the SDC powders using a co-pressing and co-sintering process; the co-sintering temperature was 1250^{o}C, and the cells based on the SDC electrolyte showed high OCV and high performance at 600^{o}C [41]. Due to the high sinterability

of the SDC powder derived from the modified GNP process, it is expected that the co-sintering temperature of the SDC electrolyte membrane may be further reduced. In this paper, we systematically studied the microstructure and electrochemical performance of the cells fabricated from the highly-active SDC powders at reduced temperatures: 1200, 1150, and 1100^{o}C.

2. Experimental

2.1 Powder synthesis

All powders involved in this work, including SDC, NiO and $Sm_{0.5}Sr_{0.5}CoO_3$ (SSC), were synthesized via GNP as described in detail elsewhere [10, 12, 41]. Taking the synthesis of SDC powders as an example, $Sm(NO_3)_3{\cdot}6H_2O$, $Ce(NO_3)_3{\cdot}6H_2O$, and $Ce(NH_4)_2(NO_3)_6$ (all from Alfa Aesar) were dissolved in distilled water with a molar ratio of 1:3:1, then glycine (Alfa Aesar) was added as both the complexing agent and the fuel with a stoichiometric glycine/nitrate ratio of 28/15 [41]. After sufficiently stirring to achieve complete complexation, the solution was heated on a hotplate till rapid self-sustaining combustion, and the resulted ashes were calcined at 600^{o}C for 2 h to form fluorite phase SDC powders. In the case of NiO and SSC synthesis, the resulted ashes were both calcined at 850^{o}C for 4 h to get the desired oxides.

2.2 Single cell fabrication

Bi-layer pellets consisting of porous NiO-SDC substrate and dense SDC electrolyte were fabricated using a co-pressing and co-sintering process [42, 43]. NiO and SDC powders were mixed together to form the precursor of the anode substrate, in which starch (Sigma) was also added as pore former to increase the porosity. The

mass ratio of NiO, SDC, and starch in the substrate was 65:35:15. The mixed powders were initially compacted at 50MPa. Then a thin layer of SDC powders were uniformly distributed onto the pre-pressed substrate and uniaxially co-pressed to 250MPa to form green bi-layer pellets. These bi-layer pellets were subsequently co-sintered at different temperatures, including 1250, 1200, 1150 and 1100^{o}C for 5 h to densify the electrolyte. The sintered anode substrate thickness and diameter were 0.48±0.01 mm and 10.8±0.2 mm, respectively, while the thickness of the electrolyte membrane was about 23.5±1.0 μm. Then, SSC and SDC powders with a mass ratio of SSC:SDC=7:3 were mixed thoroughly with an organic binder (V-006, Heraeus) to form the cathode slurry, which was subsequently screen-printed onto the electrolyte surface of the sintered bi-layer pellets, followed by firing at 950^{o}C for 2h. The effective cathode area was 0.3 cm^2, and the whole process was kept as consistent as possible so that identical cathode polarization resistance could be achieved. For brevity, the cells with anode and electrolyte co-sintered at various tempeatures are named as Cell-1250, Cell-1200, Cell-1150 and Cell-1100 thereafter.

2.3 Cell testing and characterization

Each single cell was sealed onto an alumina tube using ceramic adhesive (Aremco, Ceramabond 552). NiO paste (Heraeus) and silver paste (Heraeus) were employed as current collector on the anode and the cathode side, respectively, and Ag wire as the lead for both electrodes. Humidified (3% H_2O) hydrogen was fed to the anode at a flow rate of 30 mL/min as the fuel, while ambient air was used as the oxidant. In addition to measuring the current-voltage curve with an Arbin fuel cell

testing system (MSTAT), the electrochemical impedance spectra were measured under open circuit conditions using an EG&G PAR potentiostat (model 273A) interface combined with a Solartron 1255 HF frequency response analyzer. The microstructures of the cells were examined using a scanning electron microscope (SEM, LEO 1530) after polishing and thermal etching at 1100^{o}C for 10min, and the porosity of the anode substrate before and after reduction was measured via the Archimedes method.

3. Results and discussions

3.1 Cell morphologies

Fig. 1 shows some typical cross-sectional views of SDC electrolyte layer of Cell-1250, Cell-1200, Cell-1150, and Cell-1100, suggesting that the SDC electrolyte layer is extremely dense, even for the sample co-sintered at only 1150^{o}C. It is noted, however, that some small pin holes are observed on the electrolyte of Cell-1100. Fortunately, these pores are largely isolated from each other so that the Cell-1100 was still air-tight for operation. Besides, the average grain size of the SDC electrolyte layer decreased as the co-sintering temperature was reduced.

The morphology of the anode is also dependent sensitively on the co-sintering temperatures. Fig. 2 presents some typical cross-sectional views of the Ni-SDC anodes of the test cells after reduction in humidified hydrogen at 600^{o}C for 2h. As expected, the grain size decreased significantly as the co-sintering temperature was reduced. The porosity of the anodes before and after reduction was measured using the Archimedes method, as plotted in Fig. 2e. When the co-sintering temperature was reduced from 1250 to 1100^{o}C, the porosity of the NiO-SDC substrate increased by

~12.4%, from 24.8±0.4% to 37.2±0.4%. After reduction at 600^{o}C for 2h, the porosity of each anodes further increased by ~19%, reaching 56.2±0.4% for Cell-1100. Higher porosity and finer grain size are very favorable for rapid fuel/product transport and electrochemical reactions, thus higher performance. Reducing the co-firing temperature would help to increase porosity while reducing grain size of the electrodes.

3.2 Cell performance at 600^{o}C

Fig 3a shows some typical current-voltage curves of the cells co-sintered at different temperatures, as tested at 600^{o}C with humidified hydrogen (3% H_2O) as fuel and ambient air as oxidant. As can be seen clearly, Cell-1250 exhibits an open circuit voltage (OCV) of ~0.901 V, a rather high value for SOFCs based on thin-film DCO electrolyte at this operation temperature [10, 44]. Moreover, a peak power density of ~0.762 Wcm^{-2} is achieved for this cell. The OCV values remained relatively constant as the co-sintering temperature was reduced to 1200 and 1150^{o}C, indicating that the SDC film was dense at these lower sintering temperatures. Besides, the output performance increased significantly as the co-sintering temperature was reduced. Cell-1200 demonstrated a peak power density of ~0.898 Wcm^{-2}, which increased to ~0.933 Wcm^{-2} for Cell-1150. It is believed that the increased performance is attributed to finer microstructure of the anode and hence larger number of active sites for electrochemical reactions [45, 46]. Further lowering the co-sintering temperature to 1100^{o}C, however, leads to a sharp decrease in both OCV and cell performance, due probably to the relatively lower density of the SDC electrolyte layer. Consequently,

1150^{o}C is an optimized co-sintering temperature for thin-film SDC based cells fabricated by this co-pressing technique. Moreover, Cell-1150 displayed good stability, as shown in Fig. 3b.

To obtain more detailed information, typical electrochemical impedance spectra are acquired under open circuit conditions with a two-electrode configuration, as shown in Fig. 4a. The ohmic resistances are obtained from the high frequency intercepts with the real axis, and the total polarization resistances R_p are determined from the following equation [47]:

$$R_p = \frac{R_t - R_\Omega}{\frac{V_{oc}}{En}[1-\frac{R_\Omega}{R_t}(1-\frac{V_{oc}}{En})]} \quad (1)$$

where E_n is the Nernst potential at 600^{o}C, V_{oc} is the measured OCV, R_Ω is the ohmic resistance, and R_t is the total resistance determined from the low frequency intercept with the real axis in the impedance spectra . R_Ω and the calculated R_p are then plotted versus the co-sintering temperature in Fig. 4b. It is seen that both R_p and R_Ω were decreased as the co-sintering temperature was reduced from 1250 to 1200 and 1150^{o}C (R_p was decreased form 0.204 to 0.180 and 0.171 Ωcm^2, respectively, while R_Ω was decreased from 0.114 to 0.107 and 0.093 Ωcm^2, respectively), due most likely to extended effective triple phase boundary (TPB) and improved anode-electrolyte interface with optimized anode microstructures [45, 46]. However, when the co-sintering temperature was further reduced to 1100^{o}C, R_Ω increased significantly due to lower density of the electrolyte membrane as shown in Fig. 1d.

3.3 Cell performance at different temperatures

The cells were also tested at 550 and 650^{o}C, as shown in Fig. 5a. It is clear that Cell-1150 showed the best performance at the all operating temperatures studied: 550, 600 and 650^{o}C. Even at 550^{o}C, a peak power density as high as 0.620 Wcm^{-2} was achieved for that cell.

Shown in Fig. 5b are some typical current-voltage curves of the cells tested at 650^{o}C. As expected, the OCVs of the cells were significantly lower than the values obtained at 600^{o}C (see Fig. 3a), due to increased electronic transference number of DCO electrolyte at higher temperatures. The OCVs of Cell-1200 and Cell-1150 are still very close to that of Cell-1250 (~0.845V), but Cell-1100 displayed a much lower OCV (~0.795 V), due to insufficient density of the DCO electrolyte membrane.

On the other hand, it is noted that Cell-1150 and Cell-1200 showed significantly higher cell performance than Cell-1250 under typical operating conditions. For example, a peak power density as high as ~1.124 Wcm^{-2} was demonstrated by Cell-1150 and ~1.076 Wcm^{-2} by Cell-1200. In contrast, Cell-1250 showed a peak power density of only ~0.862 Wcm^{-2}. It appears that the increased porosity of the anodes co-fired at lower temperatures may facilitate the rate of the electrochemical processes and enhanced the cell performance. In addition, it is found that the electrode polarization at high current densities is significantly suppressed when the co-sintering temperature is reduced.

4. Conclusion

In summary, we have successfully fabricated high-performance, single cells by co-pressing followed by co-sintering at a temperature as low as 1150^{o}C using

highly-active SDC powders derived from a modified glycine-nitrate process, which uses 75 mol% $Ce(NO_3)_3$ and 25 mol% $Ce(NH_4)_2(NO_3)_6$ as a mixed cerium source. In particular, the low firing temperature has resulted in anode microstructures with more appropriate porosity, grain size, and connectivity with the electrolyte, significantly reducing both the ohmic resistance and the electrode polarization and enhancing cell performance.

Acknowledgement

This material is based upon work supported as part of the Heterogeneous Functional Materials (HetroFoaM) Center, an Energy Frontier Research Center funded by the U.S. Department of Energy, Office of Science, Office of Basic Energy Sciences under Award Number DE-SC0001061. Zhangbo Liu acknowledges a fellowship from the China Scholarship Council.

References

1. **Steele, B.C.H. and Heinzel A., *Materials for fuel-cell technologies.* Nature, 2001. 414(6861): p. 345-352.**
2. **Zhan, Z.L. and Barnett S.A., *An Octane-Fueled Solid Oxide Fuel Cell.* Science, 2005. p. 844-847.**
3. **Huang, Y.H., et al., *Double Perovskites as Anode Materials for Solid-Oxide Fuel Cells.* Science, 2006. p. 254-257.**
4. **Yang, L., et al., *Enhanced Sulfur and Coking Tolerance of a Mixed Ion Conductor for SOFCs: $BaZr_{0.1}Ce_{0.7}Y_{0.2-x}Yb_xO_{3-\delta}$.* Science, 2009. p. 126-129.**
5. **Cheng, Z., et al., *From Ni-YSZ to sulfur-tolerant anode materials for SOFCs: electrochemical behavior, in situ characterization, modeling, and future perspectives.* Energy & Environmental Science, 2011. 4(11): p. 4380-4409.**
6. **Liu, M., et al., *Rational SOFC material design: new advances and tools.* Materials Today, 2011. 14(11): p. 534-546.**
7. **Liu, M., et al., *Direct octane fuel cells: A promising power for transportation.* Nano Energy, 2012. 1(3): p. 448-455.**
8. **Brett, D.J.L., et al., *Intermediate temperature solid oxide fuel cells.* Chemical Society Reviews, 2008. 37(8): p. 1568-1578.**
9. **Jiang, Z., et al., *Nano-structured composite cathodes for intermediate-temperature solid***

oxide fuel cells via an infiltration/impregnation technique. **Electrochimica Acta, 2010. 55(11): p. 3595-3605.**

10. **Liu, Z., et al.,** ***Effect of impregnation phases on the performance of Ni-based anodes for low temperature solid oxide fuel cells.*** **Journal of Power Sources, 2011. 196(20): p. 8561-8567.**
11. **Shao, Z., et al.,** ***Advanced synthesis of materials for intermediate-temperature solid oxide fuel cells.*** **Progress in Materials Science, 2012. 57(4): p. 804-874.**
12. **Xia, C., et al.,** ***$Sm_{0.5}Sr_{0.5}CoO_3$ cathodes for low-temperature SOFCs.*** **Solid State Ionics, 2002. 149(1-2): p. 11-19.**
13. **Fu, C., et al.,** ***Electrochemical characteristics of LSCF-SDC composite cathode for intermediate temperature SOFC.*** **Electrochimica Acta, 2007. 52(13): p. 4589-4594.**
14. **Pérez-Coll, D., et al.,** ***Reducibility of $Ce_{1-x}Gd_xO_{2-\delta}$ in prospective working conditions.*** **Journal of Power Sources, 2007. 173(1): p. 291-297.**
15. **Ding, D., et al.,** ***High reactive $Ce_{0.8}Sm_{0.2}O_{1.9}$ powders via a carbonate co-precipitation method as electrolytes for low-temperature solid oxide fuel cells.*** **Solid State Ionics, 2008. 179(21-26): p. 896-899.**
16. **Ding, C., et al.,** ***Preparation of Doped Ceria Electrolyte Films for SOFCs by Spray Coating Method.*** **Journal of Dispersion Science and Technology, 2009. 30(2): p. 241-245.**
17. **Ding, D., et al.,** ***Electrical properties of samaria-doped ceria electrolytes from highly active powders.*** **Electrochimica Acta, 2010. 55(15): p. 4529-4535.**
18. **Gaudillere, C., et al.,** ***Screening of ceria-based catalysts for internal methane reforming in low temperature SOFC.*** **Catalysis Today, 2010. 157(1-4): p. 263-269.**
19. **Kudo, T. and Obayashi H.,** ***Oxygen Ion Conduction of Fluorite-Type $Ce_{1-X}Ln_xO_{2-X/2}$ (Ln= Lanthanoid Element).*** **Journal of the Electrochemical Society, 1975. 122(1): p. 142-147.**
20. **Gerhardt-Anderson, R. and Nowick A.S.,** ***Ionic conductivity of CeO_2 with trivalent dopants of different ionic radii.*** **Solid State Ionics, 1981. 5(0): p. 547-550.**
21. **Yahiro, H., et al.,** ***High-Temperature Fuel-Cell with Ceria-Yttria Solid Electrolyte.*** **Journal of the Electrochemical Society, 1988. 135(8): p. 2077-2080.**
22. **Kleinlogel, C. and Gauckler L.J.,** ***Sintering and properties of nanosized ceria solid solutions.*** **Solid State Ionics, 2000. 135(1-4): p. 567-573.**
23. **Kleinlogel, C. and Gauckler L.J.,** ***Sintering of Nanocrystalline CeO_2 Ceramics.*** **Advanced Materials, 2001. 13(14): p. 1081-1085.**
24. **Zhang, T.S., et al.,** ***Effect of transition metal oxides on densification and electrical properties of Si-containing $Ce_{(0.8)}Gd_{(0.2)}O_{(2-delta)}$ ceramics.*** **Solid State Ionics, 2004. 168(1-2): p. 187-195.**
25. **Yoshida, H. and Inagaki T.,** ***Effects of additives on the sintering properties of samaria-doped ceria.*** **Journal of Alloys and Compounds, 2006. 408-412(0): p. 632-636.**
26. **Zhang, T.S., et al.,** ***Preparation and properties of dense $Ce_{0.9}Gd_{0.1}O_{2-delta}$ ceramics for use as electrolytes in IT-SOFCs.*** **Journal of Alloys and Compounds, 2006. 422(1-2): p. 46-52.**
27. **Zhang, X., et al.,** ***A study on sintering aids for $Sm_{0.2}Ce_{0.8}O_{1.9}$ electrolyte.*** **Journal of Power Sources, 2006. 162(1): p. 480-485.**
28. **Nicholas, J.D. and De Jonghe L.C.,** ***Prediction and evaluation of sintering aids for Cerium Gadolinium Oxide.*** **Solid State Ionics, 2007. 178(19-20): p. 1187-1194.**
29. **Fu, C.J., et al.,** ***Effects of transition metal oxides on the densification of thin-film GDC***

electrolyte and on the performance of intermediate-temperature SOFC. **International Journal of Hydrogen Energy, 2010. 35(20): p. 11200-11207.**

30. **Han, M., et al.,** ***Influence of Lithium Oxide Addition on the Sintering Behavior and Electrical Conductivity of Gadolinia Doped Ceria.*** **Journal of Materials Science & Technology, 2011. 27(5): p. 460-464.**
31. **Zheng, Y., et al.,** ***Effect of Sr on Sm-doped ceria electrolyte.*** **International Journal of Hydrogen Energy, 2011. 36(8): p. 5128-5135.**
32. **Li, S., et al.,** ***Feasibility and mechanism of lithium oxide as sintering aid for $Ce_{0.8}Sm_{0.2}O$ delta electrolyte.*** **Journal of Power Sources, 2012. 205: p. 57-62.**
33. **VanHerle, J., et al.,** ***Low temperature fabrication of (Y,Gd,Sm)-doped ceria electrolyte.*** **Solid State Ionics, 1996. 86-8: p. 1255-1258.**
34. **Torrens, R.S., et al.,** ***Characterisation of $(CeO_2)_{0.8}(GdO_{1.5})_{0.2}$ synthesised using various techniques.*** **Solid State Ionics, 1998. 111(1-2): p. 9-15.**
35. **Dikmen, S., et al.,** ***Hydrothermal synthesis and properties of $Ce_{1-x}Gd_xO_{2-\delta}$ solid solutions.*** **Solid State Sciences, 2002. 4(5): p. 585-590.**
36. **Ruiz-Trejo, E., et al.,** ***Microstructure and electrical transport in nano-grain sized $Ce_{0.9}Gd_{0.1}O_{2-delta}$ ceramics.*** **Journal of Solid State Chemistry, 2007. 180(11): p. 3093-3100.**
37. **Fuentes, R.O. and Baker R.T.,** ***Synthesis and properties of Gadolinium-doped ceria solid solutions for IT-SOFC electrolytes.*** **International Journal of Hydrogen Energy, 2008. 33(13): p. 3480-3484.**
38. **Prasad, D.H., et al.,** ***Synthesis of nano-crystalline $Ce_{0.9}Gd_{0.1}O_{1.95}$ electrolyte by novel sol-gel thermolysis process for IT-SOFCs.*** **Journal of the European Ceramic Society, 2008. 28(16): p. 3107-3112.**
39. **Moure, A., et al.,** ***Synthesis, sintering and electrical properties of yttria-calcia-doped ceria.*** **Journal of the European Ceramic Society, 2009. 29(12): p. 2559-2565.**
40. **Jung, W.S., et al.,** ***Lowering the sintering temperature of Gd-doped ceria by mechanochemical activation.*** **Ceramics International, 2010. 36(1): p. 371-374.**
41. **Liu, Z., et al.,** ***Highly active $Sm_{0.2}Ce_{0.8}O_{1.9}$ powders of very low apparent density derived from mixed cerium sources.*** **Journal of Power Sources, 2013. 229(1): p. 277-284.**
42. **Xia, C. and Liu M.,** ***A Simple and Cost-Effective Approach to Fabrication of Dense Ceramic Membranes on Porous Substrates.*** **Journal of the American Ceramic Society, 2001. 84(8): p. 1903-1905.**
43. **Xia, C. and Liu M.,** ***Low-temperature SOFCs based on $Gd_{0.1}Ce_{0.9}O_{1.95}$ fabricated by dry pressing.*** **Solid State Ionics, 2001. 144(3-4): p. 249-255.**
44. **Zhang, X., et al.,** ***$Sm_{0.5}Sr_{0.5}CoO_3$+$Sm_{0.2}Ce_{0.8}O_{1.9}$ composite cathode for cermet supported thin $Sm_{0.2}Ce_{0.8}O_{1.9}$ electrolyte SOFC operating below 600^oC.*** **Journal of Power Sources, 2006. 160(2): p. 1211-1216.**
45. **Suzuki, T., et al.,** ***Impact of Anode Microstructure on Solid Oxide Fuel Cells.*** **Science, 2009. 325(5942): p. 852-855.**
46. **Gamble, S.,** ***Fabrication-microstructure-performance relationships of reversible solid oxide fuel cell electrodes-review.*** **Materials Science and Technology, 2011. 27(10): p. 1485-1497.**
47. **Liu, M. and Hu H.,** ***Effect of Interfacial Resistance on Determination of Transport Properties of Mixed-Conducting Electrolytes*****. Journal of the Electrochemical Society, 1996. p. L109-L112.**

Figure Captions

Fig. 1 Cross-sectional views of SDC electrolyte layer of a) Cell-1250, b) Cell-1200, c) Cell-1150 and d) Cell-1100.

Fig.2 Cross-sectional views of Ni-SDC anodes of a) Cell-1250, b) Cell-1200, c) Cell-1150 and d) Cell-1100 after reduction at 600^{o}C for 2h, (e) porosity of these anodes before and after reduction measured by the Archimedes method.

Fig. 3 (a) Dependence of cell voltage and power density on current density for various cells, and (b) current density as a function of time at a constant voltage of 0.5 V for Cell-1150 at 600^{o}C, when humidified H_2 (3% H_2O) and ambient air are used as the fuel and the oxidant, respectively.

Fig. 4 (a) Impedance spectra measured under open circuit conditions, and (b) calculated R_Ω and R_p, for various cells at 600^{o}C.

Fig. 5 (a) Peak power density measured at different temperatures, and (b) dependence of cell voltage and power density on current density at 650^{o}C for various cells, when humidified H_2 (3% H_2O) and ambient air are used as the fuel and the oxidant, respectively.

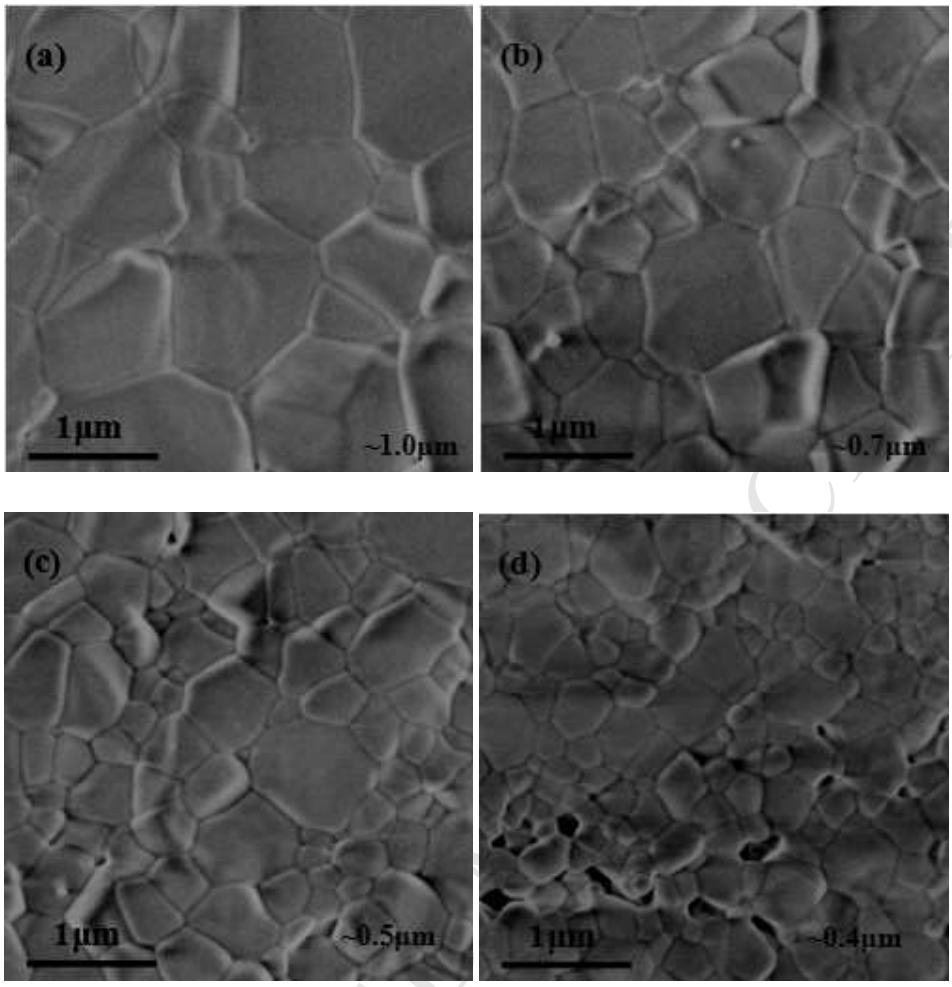

Fig. 1

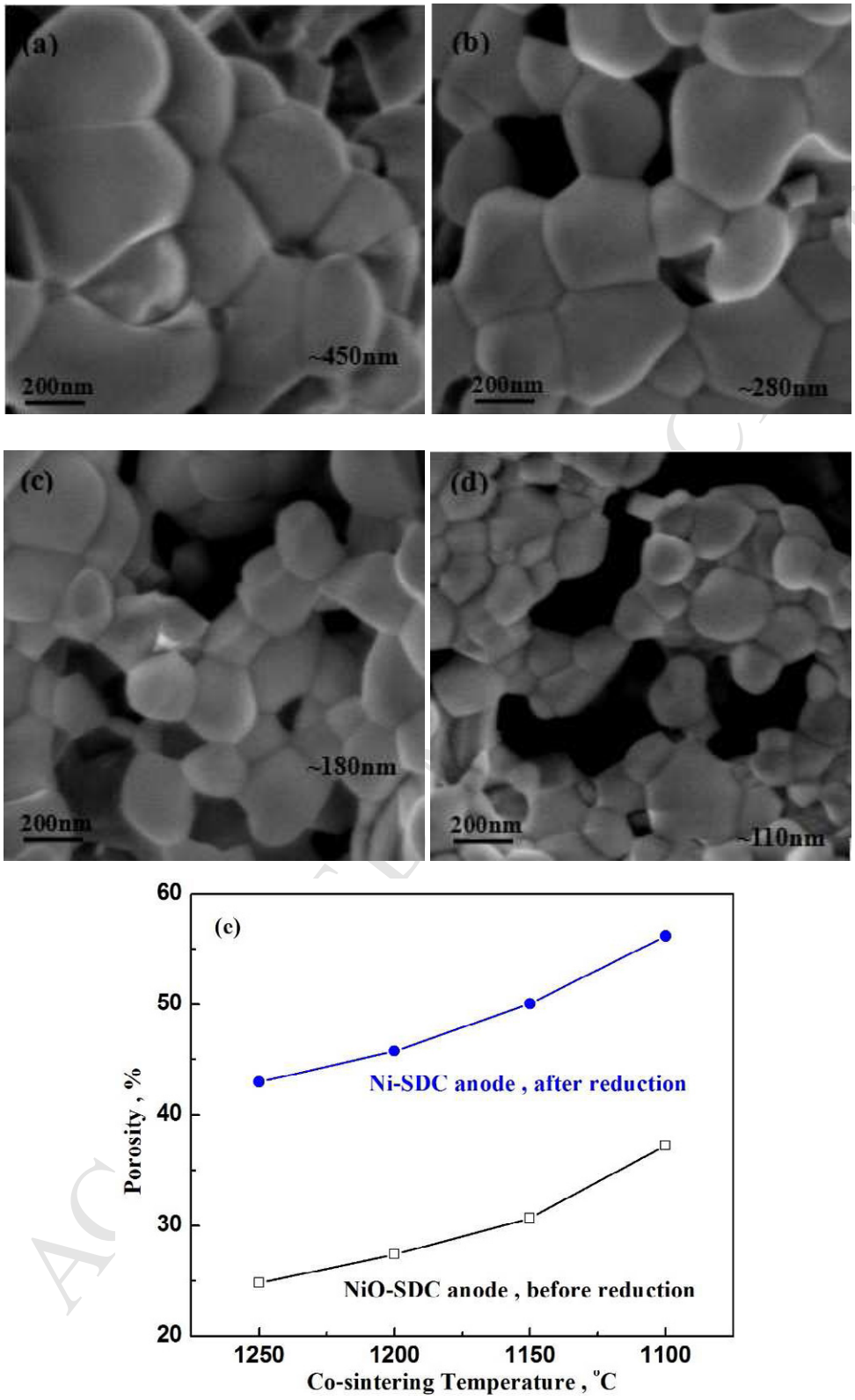
(a)
~450nm
200nm
(b)
200nm
~280nm
(c)
~180nm
200nm
(d)
200nm
~110nm
(c)
Ni-SDC anode , after reduction
NiO-SDC anode , before reduction
Porosity , %
Co-sintering Temperature , °C
60
50
40
30
20
1250
1200
1150
1100

Fig. 2

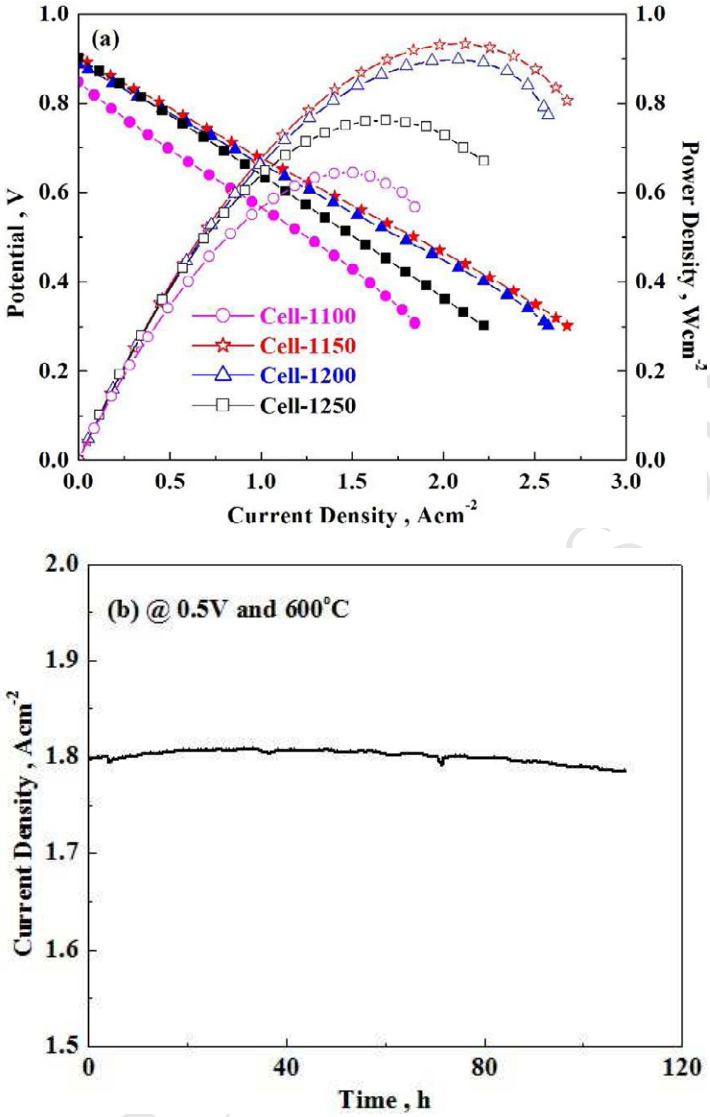
(a)
Potential , V
Power Density , Wcm-2
Current Density , Acm-2
Cell-1100
Cell-1150
Cell-1200
Cell-1250
(b) @ 0.5V and 600°C
Current Density , Acm-2
Time , h

Fig. 3

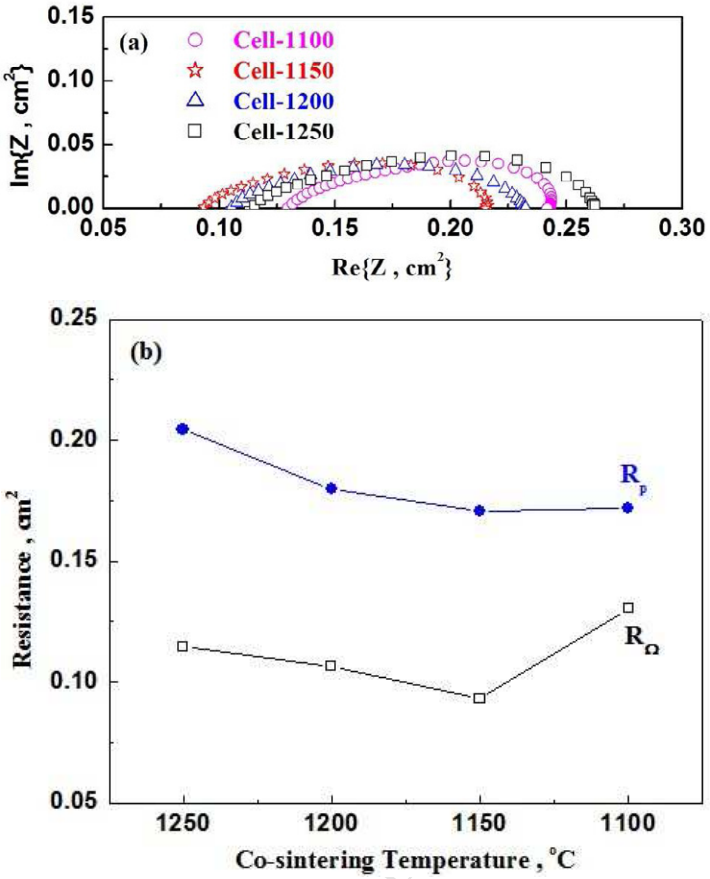

Fig. 4

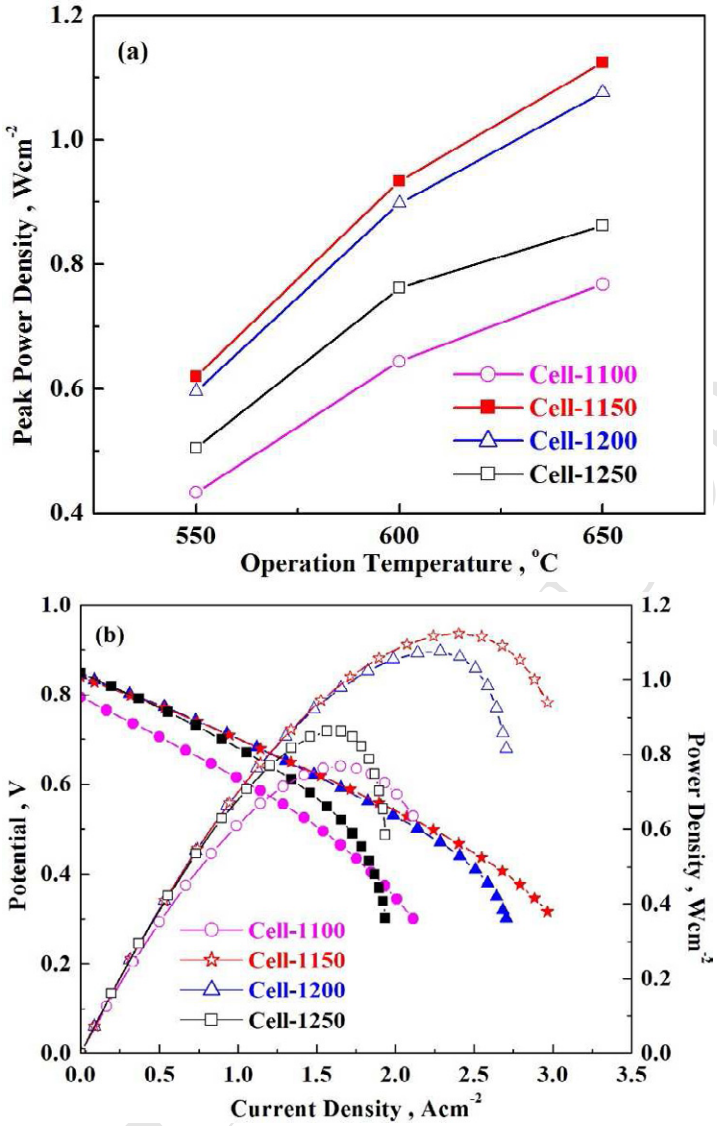
(a)
Peak Power Density , Wcm-2
Operation Temperature , °C
Cell-1100
Cell-1150
Cell-1200
Cell-1250
(b)
Potential , V
Power Density , Wcm-2
Current Density , Acm-2

Fig. 5